Int J Mater Form (2015) 8:455–468
DOI 10.1007/s12289-014-1189-4

ORIGINAL RESEARCH

# Experimental contribution to the study of the Ti6Al4V chip formation in orthogonal cutting on a milling machine

**F. Ducobu · E. Rivière-Lorphèvre · E. Filippi**

Received: 28 April 2014 / Accepted: 28 August 2014 / Published online: 16 September 2014


**Abstract** Machining by removing chips with a cutting tool is a complex operation involving many phenomena. Ti6Al4V chip formation, and particularly when it is saw-toothed (or segmented), still needs to be investigated numerically and experimentally to understand the mechanisms it involves. The use of numerical modeling has been increasingly growing since the last decade but experiments remain essential to validate the models. These two approaches are complementary and closely linked. Experiments are, however, time consuming and often difficult to implement. Moreover, orthogonal cutting as a method should be employed as to compare with the modelings. This paper presents a novel setup to perform strictly orthogonal cutting experiments with a milling machine at cutting speeds of up to 30 m/min. The configuration adopted does not require the machine tool to be modified and the small dimensions of the sample limit the costs linked to the workpiece material. The experiments, performed with the titanium alloy Ti6Al4V, constitute the basis of a benchmark for numerical orthogonal cutting validation based on chip morphology (without chip distortion due to unrolling), mechanism of chip formation, cutting forces and teeth formation frequency. The experimental results of this study highlight that the formation of a saw-toothed chip is due to the deformation and the propagation of a crack inside the primary shear zone for the cutting conditions of this paper. They also show that there is no material between the teeth on the lateral faces of the chip and that the FFT of the roughness of the machined surface is a good estimator for the teeth formation frequency.

F. Ducobu (✉) · E. Rivière-Lorphèvre · E. Filippi
University of Mons (UMONS), Faculty of Engineering (FPMs), Machine Design and Production Engineering Department, 20 Place du Parc, 7000 Mons, Belgium
e-mail: Francois.Ducobu@umons.ac.be

**Keywords** Benchmark · Chip formation · Experiments · Milling machine · Orthogonal cutting · Titanium alloy Ti6Al4V

## Introduction

Titanium and its alloys are widely used in the biomedical sector to produce implants, stents or tools for surgery and in the dental field [7]. In 2003, more than 1000 tons of titanium prostheses were implanted worldwide [29]. Consequently, the demand for titanium machined products is expanding. According to the French Titanium Association [30], titanium is an expensive and underutilized material despite its excellent properties: the annual world production of titanium is around 80,000 tons while the production of magnesium and aluminum stands at 860,000 tons and 33 million tons respectively. This is partly due to the fact that the titanium and its alloys are considered difficult-to-machine materials because of their properties.

A high cutting speed leads to the formation of a saw-toothed chip (in the literature, this is also called segmented, serrated or fragmented) [33]. It induces vibrations during the cut, in addition to the large amount of heat generated at the tool – chip interface [17, 26]. This decreases the surface quality and the accuracy of the machined part, but also the tool life, resulting in a limited material removal rate, and consequently a low productivity [17, 26, 33]. Ti6Al4V chip formation, and particularly the saw-toothed one, therefore needs to be investigated. This issue can be addressed from two points of view: the experimental and the numerical ones. Experiments are expensive and often difficult to implement, while numerical modeling is a complement and an attractive alternative yet needs experimental results to validate the developed models.

The purpose of this paper is to provide experimental results of strictly orthogonal cutting of Ti6Al4V in order to have experimental results to validate the numerical models. It should also enable a better comprehension of saw-toothed Ti6Al4V chip formation in orthogonal cutting. For this purpose, novel experiments were set up with the constraint being that the cutting had to be strictly orthogonal while limiting the costs of their implementation to a minimum. The required quantity of Ti6Al4V was also very limited thanks to samples of small dimensions.

## Machined material: titanium alloy Ti6Al4V

Titanium is found in two crystalline forms: $\alpha$ and $\beta$ [15, 20], corresponding to two microstructures. Below approximately 882 °C, its crystallographic structure is hexagonal close-packed and is called $\alpha$. Above this temperature, the structure is body-centered cubic, due to an allotropic transformation, and is called $\beta$ [16, 18, 20]. For titanium alloys, the transition temperature (called $\beta$ transus) varies considerably depending on the alloying elements [7, 8, 15, 20], depending on the phase they stabilize.

Notable general characteristics of titanium alloys are a low density (about 60 % of steel) for a high yield strength until approximately 550–600 °C and good cryogenic properties [7]. They have an exceptional resistance to corrosion in sea water and the human body. Titanium is therefore one of the most biocompatible metals with gold and platinum. It is thus an ideal material for prostheses.

Ti6Al4V is the most widely used titanium alloy, according to [9, 16, 18, 30] among others. It is mainly composed of 6 % aluminum and 4 % vanadium in mass [20], explaining its name.

Many various microstructures can be obtained by acting on the $\alpha$ phase fraction, its morphology and its particle size [7, 18]. At room temperature, Ti6Al4V is composed of 90 % in volume of the $\alpha$ phase. It therefore dominates the physical and mechanical properties of this alloy. The microstructure also depends on the history of the forming and heat treatments [28].

Ti6Al4V is mainly used in the annealed state. Annealing, according to AMS 4928 standard, involves maintaining a temperature between 700 °C and 785 °C for one hour. Slow cooling is then required to obtain a practically stable structure [8]. Annealing generally leads to a good ductility and toughness, a high structural and dimensional stability, a relatively good machinability and a reasonable conformability [8].

For the cutting experiments of this study, Ti6Al4V grade 5 (ASM 4928) at the classic state used in the aerospace industry was chosen. It was annealed at 750 °C for one hour followed by air cooling. The main properties of annealed Ti6Al4V according to AMS 4928 standard are available in [20].

Due to these properties, Ti6Al4V machining is expensive and time consuming: the cutting forces and temperature are high, as well as the level of tool vibrations and wear [4, 13]. The tool vibrations and wear are mainly due to the formation of saw-toothed chips occurring in some cutting conditions. The high temperature at the tool – chip interface due to the specific heat and conductivity values also acts highly on the tool wear. In order to improve Ti6Al4V machinability, it is essential to understand the formation mechanisms of a saw-toothed chip. In the literature, this problem is still on-going, whether experimentally or numerically through the development of finite elements models.

Ducobu et al. [12] review the different theories found in the literature to explain the formation of this kind of chip. The first one is the adiabatic shear band [3, 14, 19, 22, 23]. Due to large shear occurring in the primary shear zone, large shear strains appear in very thin bands. This localization induces a very large temperature increase causing thermal and strain softening of the material. This thermoplastic instability (competition between hardening and strain softening) results in the formation of an adiabatic shear band. The second theory is the crack propagation [17, 31]. Due to the large shear in the primary shear zone, a continuous crack appears at the free surface of the chip and propagates to the tool. The last theory is the combination of the two previous ones in which the adiabatic shear band is the precursor of the material failure and the crack propagation [2, 5, 23]. The adiabatic shear band theory seems to be the most likely according to the recent literature [32].

## Experimental setup

Machining by removing chips with a cutting tool is a three-dimensional operation whose complex study involves many phenomena. In order to reduce the size of the models and the number of the phenomena to take into account, the orthogonal cutting is often adopted. It can be reduced to a bi-dimensional problem in a plane perpendicular to the cutting edge. The plane strain assumption is often adopted. This hypothesis is licit only when the width of cut is large compared to the depth of cut (ratio of minimum three).

### Classic orthogonal cutting configurations

To get as close as possible to the assumptions of orthogonal cutting with a turning operation, two alternatives are usually considered:

- Altintas [1] performs face turning of the end of a tube with a large diameter and a small thickness. The width of the tool is larger than the thickness of the tube.
- Mahnama and Movahhedy [21] carry out plunge turning of large diameter radial grooves having a width smaller than that of the tool.

The second method is often used because it allows to perform one experiment per groove (Fig. 1) and thus several tests on a single part. In this configuration, the numerical command of the lathe is set to "constant surface speed", G-code G96 (the rotation speed is increased progressively during the operation as the diameter decreases). The radius of the sample influences the cutting due to the curvature of the surface to machine. This takes importance when the depth of cut decreases. It cannot be neglected anymore for small depths of cut (or the radius of the sample should increase dramatically) and the process moves away from orthogonal conditions. For the tube, the machined surface is always the same and the tool erases it at each test, which makes its availability for future investigations impossible. Moreover, face turning must be done to prepare the surface to machine before each test and it is not easy to find Ti6Al4V tubes (the sample would therefore be a cylinder machined to be a tube which is not an economical solution).

## Proposition of a novel configuration

The proposed configuration uses a five-axis high speed milling machine Deckel-Maho DMU-80T. This precision milling machine ensures a high rigidity of the setup and a good positioning accuracy (around 1 $\mu$m). The main principle of the configuration is to use the milling machine as a planning machine. As shown in Fig. 2, the sample is inserted into the spindle and the tool is fixed with a custom made support piece on the force sensor which is itself on the machine table. The cutting movement is generated by the sample horizontal displacement with respect to the stationary tool (Fig. 3). In these conditions, the cutting is really orthogonal.

It must be noted that orthogonal cutting configuration could also be obtained on planning (or shaping) machines, given that the milling machine is used as a planning machine in the proposed setup. Two main reasons lead to choosing a milling machine over a planning machine. Firstly, milling machines are much more common than planning machines and, secondly, two custom made support pieces (one for the tool and one for the sample) should be used instead of only one (for the tool) in the proposed configuration, making it harder and slower to implement.

The tests aim to remove a layer of material of variable thickness (from several $\mu$m to less than 1 mm). In this paper,

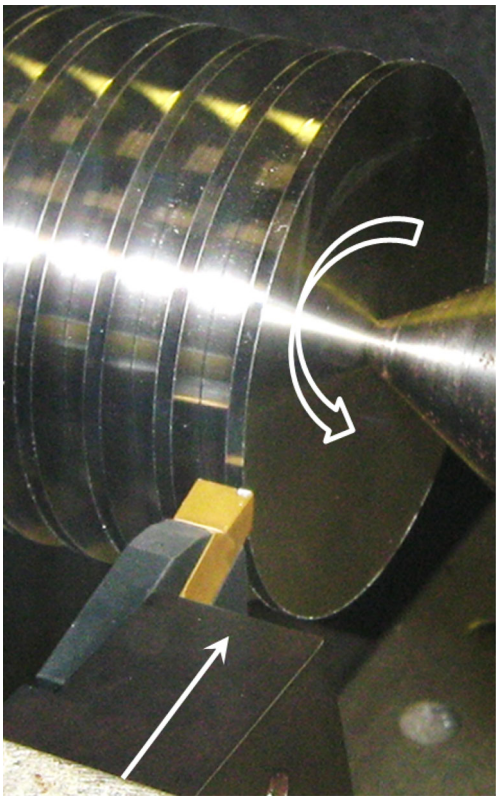

**Fig. 1** Orthogonal cutting configuration with feed direction and rotation of the sample

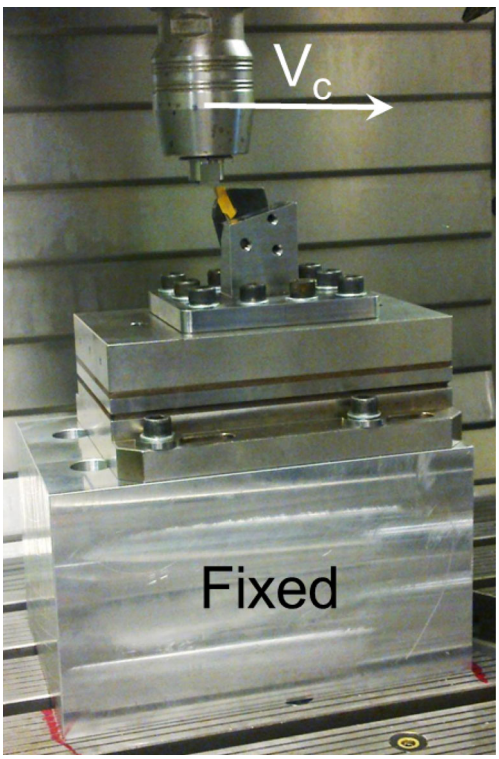


**Fig. 2** Cutting configuration

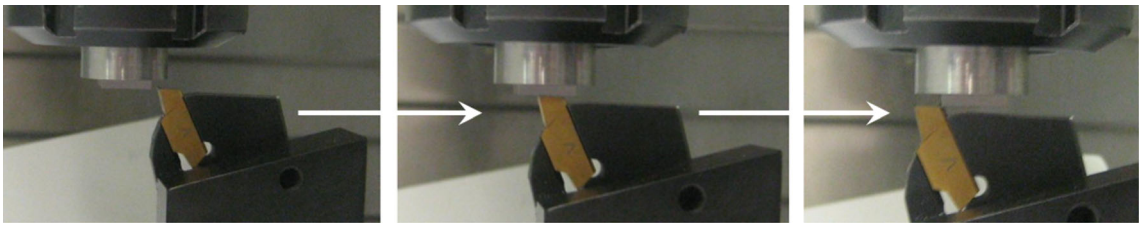

**Fig. 3** Cutting movement

the depth of cut, $h$, will remain in the macro-cutting domain (the depth of cut is larger than the tool edge radius).

The drawback of this configuration is that the maximum cutting speed is the maximum feed rate of the machine, 30 m/min in this case. This cutting speed is, however, in the range recommended by SECO for the standard tool and Ti6Al4V (27-39 m/min) [25]. This configuration is therefore suitable for this tool-material couple but the limited achievable cutting speed prevents it from being used with any material, such as an aluminum alloy for example.

Moreover, as the machine acceleration is limited, care should be taken to place the tool so that the desired speed is reached before the cut (and prior to the speed decrease when approaching the end of the axis). This has been confirmed with a Photron FASTCAM SA3 high speed camera by counting the number of frames during the cut at an acquisition frequency of 30,000 frames/s. The mean speed on the cutting length for all the tests performed in this study is 29.65 m/min with a standard deviation of 0.09 m/min. The difference with the theoretical speed (30 m/min) is 1 %, which is very low. The experimental setup is therefore validated for the cutting speed.

## Sample

The geometry of the sample is presented in Fig. 4. The sample is a cylinder of 18 mm in diameter and a minimum of 20 mm in length. Its functional part consists of three parallel tenons of 1 mm wide, 10 mm long and 2 mm high. The space between two of them (4 mm) is sufficient to prevent the tool from machining two tenons at once, assuming that it is centered on the tenon (the tool width is 6 mm, larger than the width of the cut in order to respect the orthogonal cutting hypothesis). Two square planes of 10 mm side and 1.5 mm depth are machined at 90°; one is parallel to the tenons.

The tenons to be machined are arranged on a cylindrical base, which is the part of the sample that is inserted into the spindle. The two planes at 90° are used to position it in the spindle and define a reference for the measurement of the sample. The first is parallel to the tenons and the second is perpendicular to the cutting speed direction.

The sample is composed of three tenons because the cutting length must be large enough for the process to be steady and the forces to be measured. As the sample is a cylinder, the space available is exploited by adding two "external" tenons next to the first "central" one. They can also be used to form a reference plane to measure the actual depth of material removed.

The width of the tenons is reduced to 1 mm to minimize the efforts in the spindle bearings. Moreover, it will directly give the forces value per mm width as in 2D plane strain numerical models. This value of the width allows a ratio larger than 3.5 with the depth of cut of 280 $\mu$m to be maintained and therefore satisfies the plane strain hypothesis widely used in finite elements models as in [5, 10, 11, 24] among many others.

The surface to machine (i.e. the upper face of the tenons) should have a low flatness deviation to remove a constant quantity of material along the cutting length. Flatness deviation of the tenons is lower than 5 $\mu$m and parallelism deviation between the plane at the bottom of the tenons and the plane formed by the three tenons is about 10 $\mu$m. These measurements were performed on a Wenzel LH 54

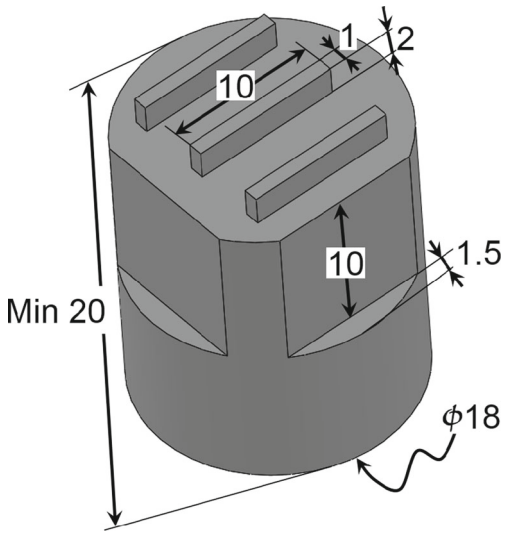


**Fig. 4** Sample *(dimensions in mm)*

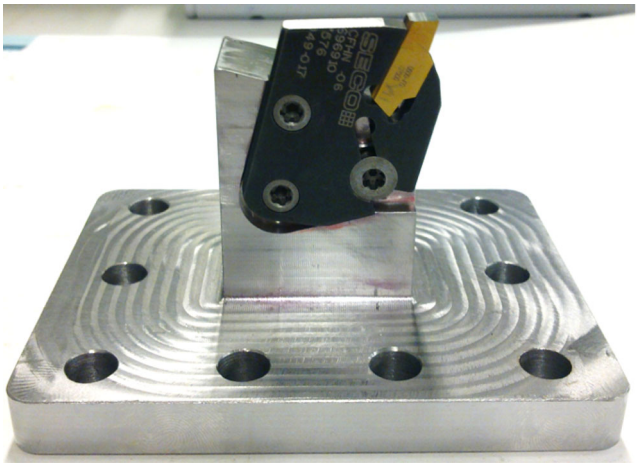

**Fig. 5** Interface part to hold the tool

Coordinate Measuring Machine (CMM) with an accuracy of approximately 3 $\mu$m.

The arithmetic roughness of the tenons has been measured with a surface roughness measurement system (Diavite DH-6) and is equal to $R_a = 0.2$ $\mu$m.

Tool

In order to place the tool on the machine table and in the proper orientation, an interface part was designed. This allows the part of the tool holder to stay in contact with the tool, and the attachment (with two screws and a third one to clamp the tool) is the same as on the original tool holder. This is presented in Fig. 5. Ten screws fix it on the force sensor.

The tool and tool holder are custom made by SECO [25] from standard elements (LCGN160602-0600-GX-X, CP500 for the tool, SFN2020NX and CFHN-06-X for the tool holder) to machine radial grooves by turning in order to provide the same characteristics as the numerical model used by Ducobu et al. [12]. The rake angle is

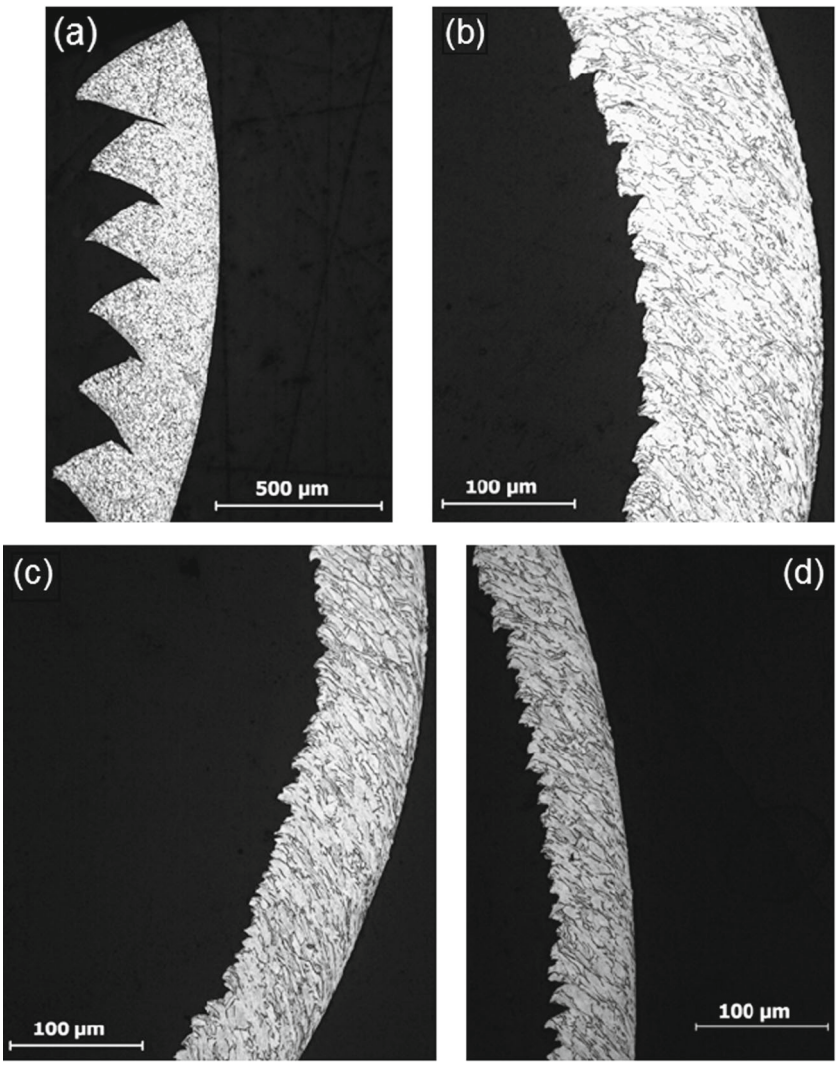


**Fig. 6** Chips on optical microscope **(a)** 280 $\mu$m, **(b)** 100 $\mu$m, **(c)** 60 $\mu$m and **(d)** 40 $\mu$m

15°, the clearance angle 2° and the cutting edge radius 20 $\mu$m.

Cutting conditions

The cutting speed is fixed at 30 m/min and remains constant for all the experiments; a test therefore takes 0.02 s since the length of the tenons is 10 mm. Four cutting conditions are considered through different values of the depth of cut: 280, 100, 60 and 40 $\mu$m. The experiments with the depths of cut of 280 $\mu$m, 100 $\mu$m, 60 $\mu$m are repeated 6 times while they are repeated 3 times for 40 $\mu$m.

Acquisition system

Cutting forces are recorded at the sampling frequency of 70 kHz with a Kistler acquisition system. It is composed of a Kistler 9257B dynamometer measuring the forces in the three directions. The signals are then amplified by the multichannel laboratory charge amplifier Kistler 5070A before passing through the data acquisition system (DAQ) Kistler 5697A2 and being recorded on a PC thanks to the DynoWare software.

## Results

Chips morphology

*Optical microscope*

Chips were collected after each test. In order to observe their cross-section with an optical microscope, the chips were embedded into epoxy resin to stand on their edge. They were then polished straight across their length. To reveal the Ti6Al4V microstructure, they were etched for about 45 s by Kroll's reagent. It colors the $\beta$ phase in dark brown (it is thus the darker color on black and white views taken with the optical microscope). Figure 6 presents the four chips with a magnification factor of 50 (a) and 200 ((b) to (d)). Only the first one is saw-toothed and its teeth seem to be overall similar. The three others can be considered as continuous chips. The last one has, however, very small and irregular teeth along its entire length.

The observations with the optical microscope allow the undeformed tooth length, $L$, the tooth height, $H$, the valley, $C$, and the pitch, $P$, to be measured for the saw-toothed chip. These lengths are highlighted in Fig. 7. It is important to note that the curvature of the chip does not affect the undeformed tooth length, unlike the pitch. The tooth height and the valley are also influenced by the curvature, but to a lesser extent.

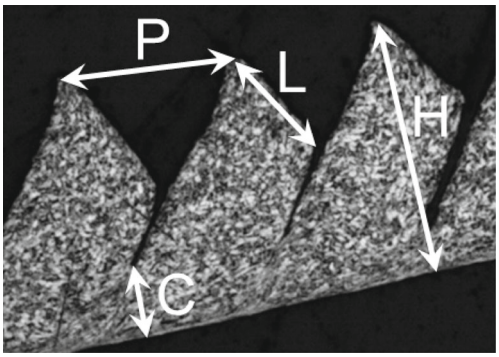


**Fig. 7** Characteristic lengths of a typical saw-toothed chip

Chips obtained with classic orthogonal cutting experiments (cf.section "Classic orthogonal cutting configurations") are usually long and rolled up and must be unrolled before embedding. Unrolling chips often leads to slightly different values for the height and the valley and, very different values for the pitch in comparison to a rolled chip. This information has never been mentioned in the literature when the chips are measured which makes it difficult to reproduce the measurement and to compare these experimental values to modeling results.

With the method developed, as the cutting length is 10 mm, the chip is too short to roll up. The chips can therefore be embedded without unrolling, and there is no error on the measured lengths due to the unrolling distortions.

Table 1 presents the mean and standard deviation values of the four lengths for 25 teeth. The standard deviation is similar for each length, except for the valley ($C$) which has a standard deviation larger than 10 % of its mean value.

Chips for depths of cut of 100 $\mu$m and 60 $\mu$m are similar in Fig. 6b and c. For a greater magnification factor, it is also noticed that their microstructures are very close to each other's and the primary shear zone is not easily identified when looking at the deformations of the grains (Fig. 8a for a depth of cut of 100 $\mu$m).

The 40 $\mu$m chip (Fig. 8b) is similar to the two previous ones although its shape is slightly more regular in the sense that there are small teeth on all of its length. Figure 8b shows that the primary shear zone is easily identified as the grains are highly deformed inside it.

For the saw-toothed chip (depth of cut of 280 $\mu$m), the grains are highly deformed in the primary shear zone and not inside the teeth (Fig. 9). This zone is wider than the

**Table 1** Characteristic lengths of the saw-toothed chip at 280 $\mu$m ($\sigma_x$: standard deviation of the length $x$)

| | $L$ | $H$ | $C$ | $P$ |
|---|---|---|---|---|
| $x$ ($\mu$m) | 206 | 288 | 157 | 233 |
| $\sigma_x$ ($\mu$m) | 17 | 14 | 21 | 17 |

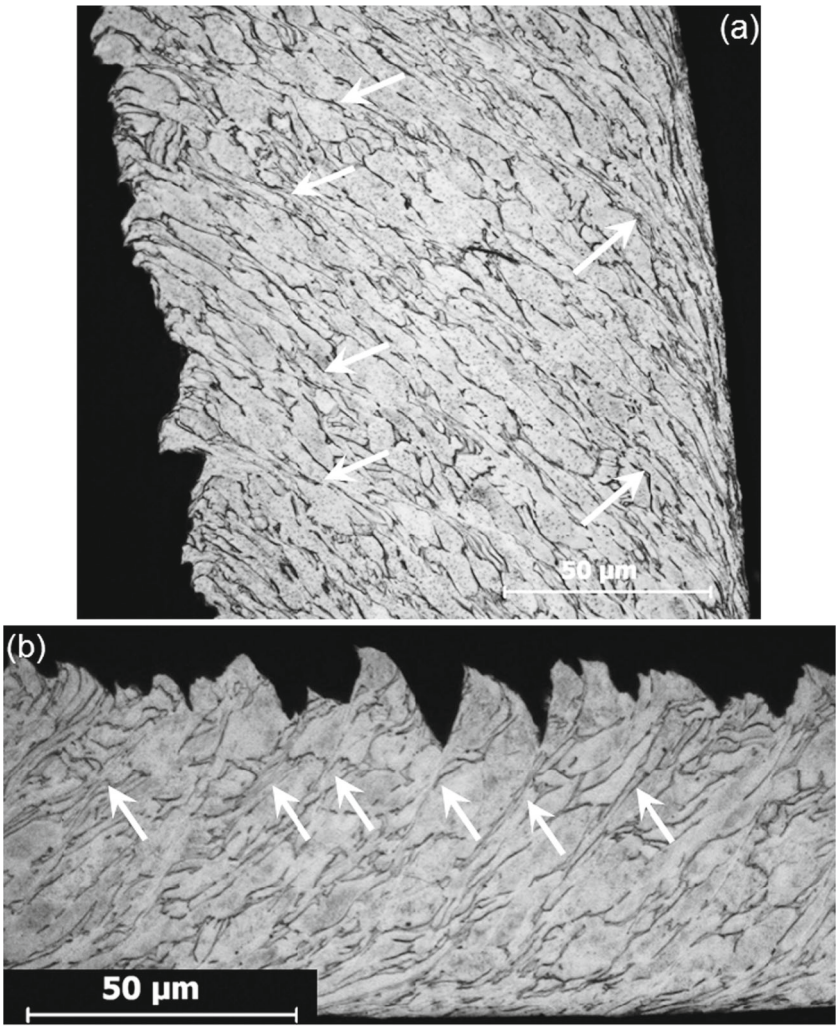


**Fig. 8** Chips microstructure at **(a)** 100 $\mu$m (*arrows point to grains deformation*) and **(b)** 40 $\mu$m *(arrows point to the primary shear zone with deformed grains)*

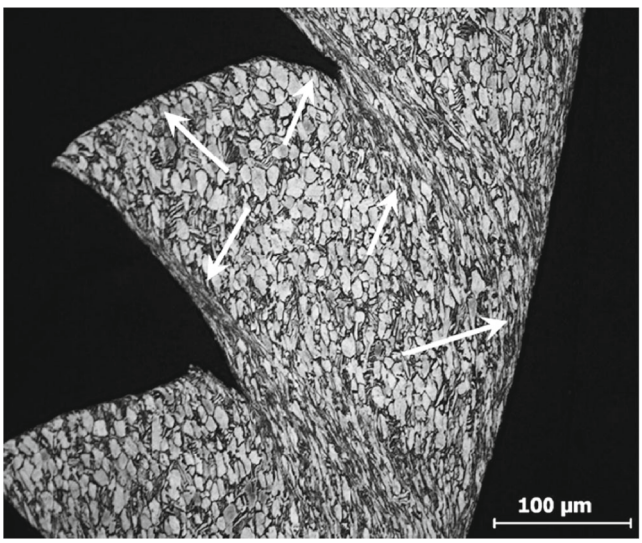


**Fig. 9** Chip microstructure for the chip at 280 $\mu$m *(arrows point to the different zones of a tooth with grains deformation of different intensities)*

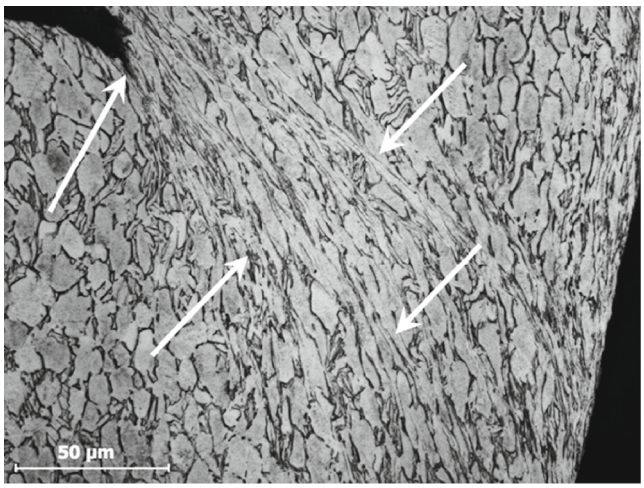


**Fig. 10** Primary shear zone for the chip at 280 $\mu$m *(arrows point to the deformed grains in the primary shear zone and the crack)*

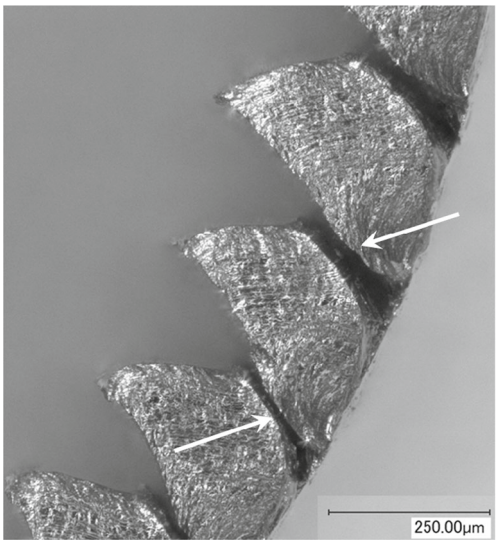


**Fig. 11** Chip for the depth of cut of 280 $\mu$m, digital microscope *(arrows point to the absence of material between two successive teeth)*

zone for the continuous chips. Deformed grains are also present on the continuous surface of the chip, which is explained by the contact with the tool and the fact that it is the area where the chip comes off the workpiece. The grains on the upper side of the teeth are also deformed but less so. This zone corresponds to the surface machined during the preparation of the sample, before the tests. Finally, on the teeth flanks, the grains are almost not deformed and the surfaces are irregular, characterizing a crack propagation.

A magnification of 500× (Fig. 10) confirms the crack propagation inside the primary shear zone, from the free surface of the chip to the tool, and that outside it the grains are not deformed. It can also be observed that the primary shear zone splits when getting near the tool. The microstructure analysis of the saw-toothed chip allows to take position relative to the different theories about the Ti6Al4V saw-toothed chip formation. It turns out that deformation and crack propagation inside the primary shear zone lead to the formation of the saw-toothed chips observed for the cutting conditions of this paper. Characteristics highlighted in the literature such as the splitting of the primary shear zone [3] are also noted.

*Digital microscope*

Chips were also observed using a Keyence VHX-2000 digital microscope. No new element appears for chips with depths of cut of 40 $\mu$m, 60 $\mu$m and 100 $\mu$m.

The observation of the 280 $\mu$m chip with this microscope, thus without embedding and polishing, reveals that its side faces are different to the central part, which is observed with the optical microscope. As Fig. 11 shows, no material is present between the teeth in the primary shear zone, and its width varies depending on the tooth considered. This absence of material can also be presumed with the naked eye. The roughness of the sides of the chip is, expectedly, high and can be observed by passing a finger over it. This aspect of saw-toothed chips cannot be observed under an optical microscope and disappears when the sample is polished. To the authors' knowledge, no information on this feature of the Ti6Al4V saw-toothed chip is found in the literature.

Cutting forces

Figure 12 shows an example of temporal evolution of the efforts during a test at the depth of cut of 280 $\mu$m. The

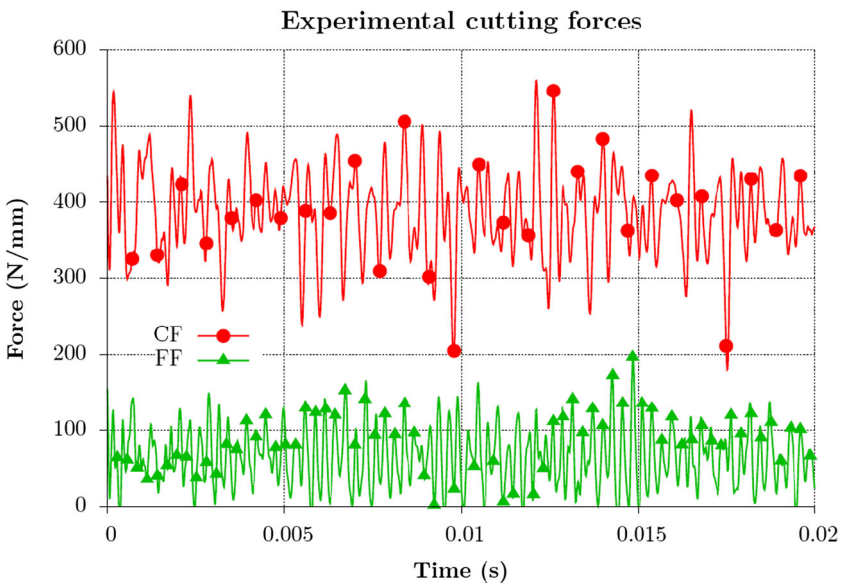


**Fig. 12** Cutting forces *(cutting force, CF, and feed force, FF)* for a cutting speed of 30 m/min and a depth of cut of 280 $\mu$m

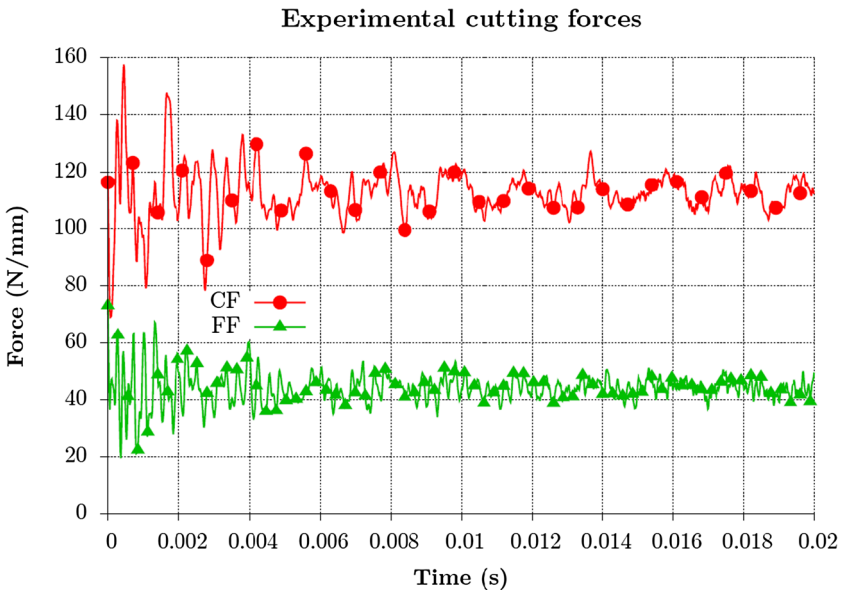


**Fig. 13** Cutting forces *(cutting force, CF, and feed force, FF)* for a cutting speed of 30 m/min and a depth of cut of 60 $\mu$m

average value of the force in the direction perpendicular to the cutting plane (not shown in Fig. 12) is zero, which confirms that the cut is orthogonal and not oblique. The two forces measured during the cut vary at a high frequency and with large amplitudes. It is not possible to identify a periodic evolution with a simple observation. This kind of cyclic evolution of the forces was expected as a saw-toothed chip is produced. When a tooth is formed, the forces decrease as the stresses in the primary shear zone are smaller. The forces then increase again with the level of stresses in the primary shear zone.

The forces are shown in Fig. 13 for the depth of cut of 60 $\mu$m. Their evolutions are similar at 40 and 100 $\mu$m. The force variations are smaller than at 280 $\mu$m and not cyclic, which is justified by the fact that the chip is continuous. As the depths of cut are smaller, a lower level of the forces was expected. At the beginning of the measurement, the forces are higher as the tool enters the workpiece, inducing a kind of impact.

The average root mean square (RMS) values of the forces for each cutting condition are summarized in Table 2. The RMS value of a quantity $x$ is calculated as follows:

$$\text{RMS of} x = \sqrt{\frac{1}{n}\sum_{i=1}^{n} x_i^2} \quad (1)$$

in which $n$ is the number of values $x_i$.

As expected, the level of the forces decreases with the depth of cut. The feed force decreases less than the cutting force when the depth of cut is smaller. The ratio of the mean RMS values ($\frac{FF}{CF}$) is also reported in the table. This ratio increases when the depth of cut decreases, showing that the tool edge radius increasingly influences the cutting process.

These results on the forces were expected, which allows to show the validity of the proposed strictly orthogonal cutting setup.

**Table 2** Cutting forces summary

| $h$ | RMS CF (N/mm) | RMS FF (N/mm) | $\frac{FF}{CF}$ |
|---|---|---|---|
| 280 ($\mu$m) | 387±2 | 77±4 | 0.20 |
| 100 ($\mu$m) | 173±2 | 51±1 | 0.29 |
| 60 ($\mu$m) | 112±2 | 45±1 | 0.40 |
| 40 ($\mu$m) | 86±2 | 41±1 | 0.48 |

## Roughness of the machined surface

The roughness of the machined surface was measured three (for 40, 60 and 100 $\mu$m) to six times (for 280 $\mu$m) for each depth of cut. Table 3 summarizes the mean values obtained for the arithmetic roughness, $R_a$.

Except for the depth of cut of 280 $\mu$m, all arithmetic roughness values are very similar and in the region of 0.09–0.10 $\mu$m. These values are very close. However, taking into account the chip morphology, it is suggested that the arithmetic roughness decreases with the depth of cut when

**Table 3** Arithmetic roughness for each depth of cut

| $h$ ($\mu$m) | 280 | 100 | 60 | 40 |
|---|---|---|---|---|
| $R_a$ ($\mu$m) | 0.692 | 0.099 | 0.086 | 0.109 |

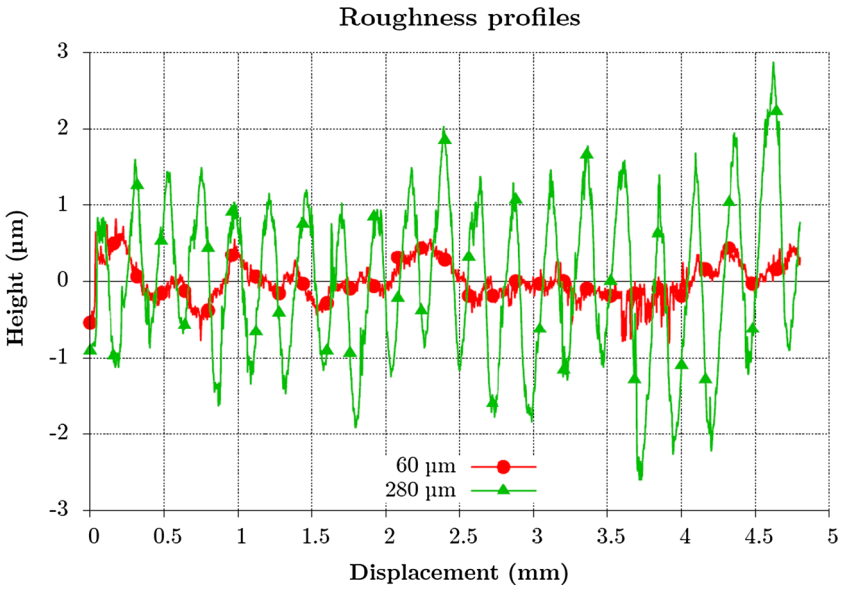


**Fig. 14** Roughness profiles for the depths of cut of 60 $\mu$m and 280 $\mu$m

the chip is continuous. The arithmetic roughness higher for 40 $\mu$m than for 60 $\mu$m could be explained by the chip at 40 $\mu$m having small and irregular teeth, inducing a decrease in the quality of the machined surface. Moreover, the influence of the cutting edge radius is higher at a depth of cut of 40 $\mu$m and ploughing has more importance than at higher depths of cut which influences the mechanism of chip formation. These results on the roughness on the machined surface were expected, which allows to show the validity of the proposed strictly orthogonal cutting setup.

The values obtained are excellent in the context of machining by removing chips. An $R_a$ of 0.80 $\mu$m is the minimum value commonly observed in milling, while an $R_a$ of 0.40 $\mu$m can be achieved [6]. In turning, the reachable value goes down to 0.20 $\mu$m [6].

Figure 14 shows examples of measured roughness profiles for the two depths of cut studied in the previous section. As for the values of the arithmetic roughness, only the profile of the largest depth of cut (280 $\mu$m) is significantly different from the others. This roughness profile results of the formation of a saw-toothed chip and presents a cyclic evolution. When looking at Figs. 12 and 14, it becomes obvious that the roughness profile and the cutting force have a similar evolution. This similitude will

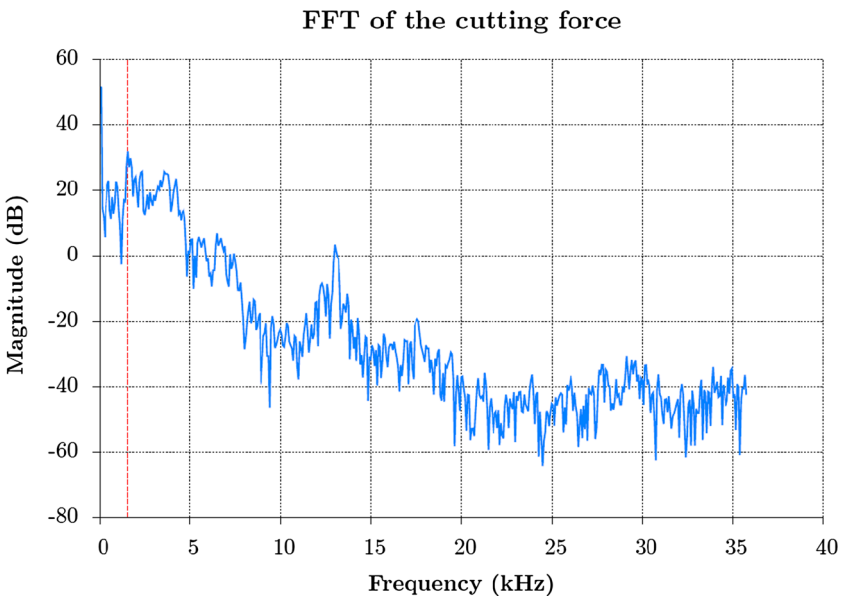


**Fig. 15** FFT of the cutting force for the depth of cut of 280 $\mu$m, highest peak highlighted

**Table 4** Summary of the values from the FFT of the cutting force

| Test | Fundamental | Highest peak | |
|---|---|---|---|
| | (N/mm) | (Hz) | (N/mm) |
| 1 | 381 | 1570 | 39.9 |
| 2 | 383.7 | 3639 | 32.4 |
| 3 | 381 | 1570 | 30.3 |
| 4 | 386.8 | 2283 | 36.6 |
| 5 | 386.5 | 1598 | 27.8 |
| 6 | 381 | 1570 | 36 |

be exploited in the next section to estimate the teeth formation frequency. As highlighted in the literature, the degradation of the surface roughness due to the production of a saw-toothed chip is another reason to avoid this kind of chip (in addition to the fatigue of the tool, whether due to cyclic variations of the forces or of the temperature on the rake face).

Teeth formation frequency

For the depth of cut of 280 $\mu$m, a saw-toothed chip is formed. The teeth formation frequency of a saw-toothed chip is often studied, as well numerically [5, 34] as experimentally [27]. The validation of a numerical model should therefore produce a chip whose teeth formation frequency is close to the experimental one. This section aims to estimate its teeth formation frequency through several ways:

- based on chip geometry;
- based on forces:
  - Fast Fourier Transform (FFT) of the cutting force signal;
  - best sine in a least squares way fitted on the cutting force evolution;
- based on the machined surface roughness.

The methods based on the machined surface roughness and the least squares are, to the authors' knowledge, not used in the literature to evaluate the teeth formation frequency.

*Estimation based on the chip geometry*

The teeth formation frequency can be estimated from the undeformed tooth length. This frequency, $f_g$, is given by [27]:

$$f_g = \frac{V_c}{L}$$

with $L$ the undeformed tooth length, measured on 25 teeth (cf. Table 1), and $V_c$ the cutting speed (30 m/min).

The undeformed tooth length is equal to 206 $\mu$m (Table 1), resulting in a frequency of 2427 Hz.

*Estimation based on the FFT*

Thanks to quite a high sampling frequency (70 kHz) and a sufficient duration of the cut (about 0.02 s), the FFT can be used to estimate the teeth formation frequency, as the frequency resolution is around 50 Hz. Standard precautions were used to limit the phenomena of aliasing and leakage, particularly through the introduction of a Hanning filter.

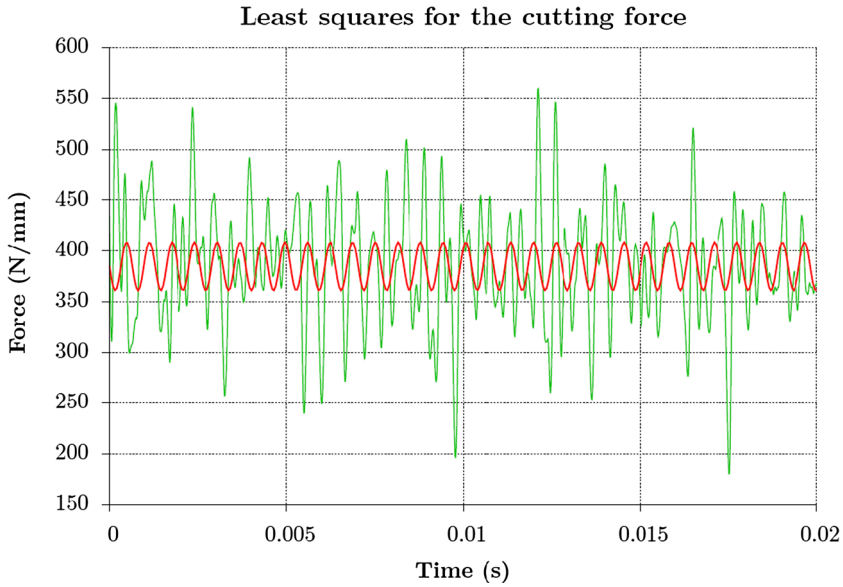


**Fig. 16** Best sine in the least squares sense for the cutting force for the depth of cut of 280 $\mu$m

**Table 5** Summary of the values from the least squares on the cutting force

| Test | DC (N/mm) | Frequency (Hz) | Amplitude (N/mm) |
|---|---|---|---|
| 1 | 385 | 1564 | 24 |
| 2 | 385 | 3622 | 24 |
| 3 | 382 | 1561 | 37 |
| 4 | 387 | 2295 | 37 |
| 5 | 387 | 1592 | 18 |
| 6 | 380 | 1557 | 21 |

Figure 15 presents the results for the cutting force of the first test. The amplitude of the fundamental frequency is 381 N/mm and corresponds to the average value of the force. The next highest peak equals 39.9 N/mm at a frequency of 1570 Hz. This corresponds to the teeth formation frequency. The proximity of the high peaks under 5 kHz makes it difficult to find which one corresponds to the formation frequency.

Table 4 shows the values for the six tests performed under these conditions. The mean value amounts to 2038 Hz with a standard deviation of 834 Hz. This is close to that obtained via the chip geometry method, but the standard deviation is high.

*Estimation based on the least squares method*

The forces evolution is now regarded as a sine of frequency equal to that of the teeth formation and whose continuous component (DC) corresponds to the average force value. The best sine in a least squares sense is therefore adjusted on the cutting force signal in this paragraph.

Figure 16 presents this sine for the first test. Its DC component (zero shift) is 385 N/mm, its amplitude 24 N/mm and its frequency 1564 Hz.

The values for the six tests are shown in Table 5. It results an average formation frequency of 2032 Hz with a standard deviation of 832 Hz. These values can be considered identical to those obtained by the FFT method. The advantage of this method over the previous one is that it provides a single frequency.

*Estimation based on the surface roughness*

Upon observing the measured roughness profiles (Fig. 14), the one corresponding to the saw-toothed chip presents a cyclic evolution which could be that of the cutting force. It is proposed to perform its FFT to evaluate the teeth formation frequency.

The length of the measured profile is 4.8 mm and 9.6 ms are needed to run through it at the cutting speed (30 m/min), leading to a frequency resolution of about 104 Hz. Figure 17 shows the results for the first measurement; the FFT is plotted to 100 kHz. Unlike the FFT of the cutting force, the main peak is clearly defined.

The mean teeth formation frequency of the measured profiles is 2082 Hz with a standard deviation of 52 Hz. This value is close to those obtained with the three previous methods and particularly these involving the cutting force, but its standard deviation is much lower, increasing confidence in the value obtained.

*Conclusions of the teeth formation frequency*

Four methods were employed to estimate the teeth formation frequency. Three of them led to nearly equal values.

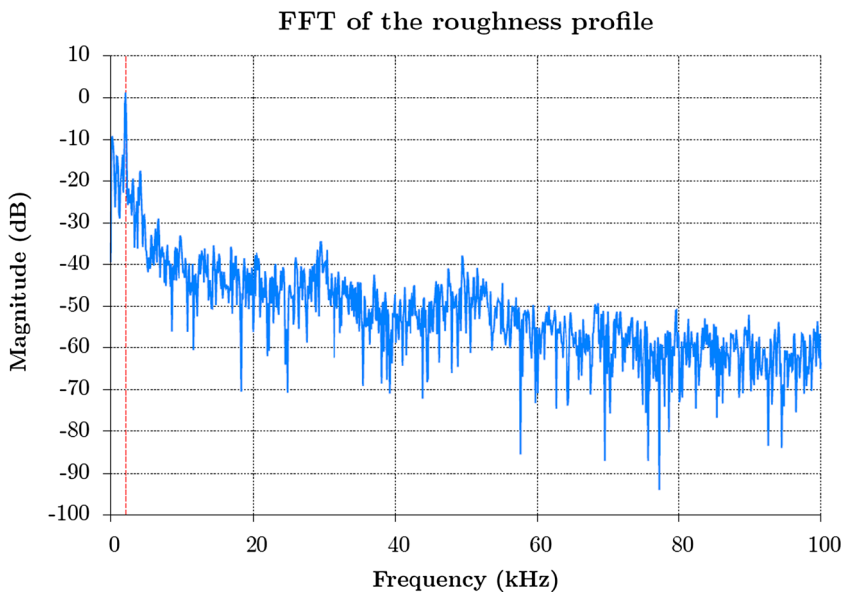


**Fig. 17** FFT of the roughness profile for the depth of cut of 280 $\mu$m *(plotted to 100 kHz)*, highest peak highlighted

The undeformed tooth length method led to a frequency slightly higher than the others. The FFT and the sine in a least squares sense methods gave the same frequency with a high standard deviation in both cases. The estimation with the FFT of the cutting force was not easy to perform as there were several high peaks after the fundamental frequency, contrary to the least squares one. The last method was based on the FFT of the roughness profile of the machined surface. This novel method led to a mean frequency identical to the previous two but with a much lower standard deviation. The peak of the frequency in this case was no longer difficult to identify.

The teeth formation frequency in orthogonal cutting at a cutting speed of 30 m/min and a depth of cut of 280 $\mu$m is therefore around 2100 Hz.

According to the results, we recommend to use the method based on the chip geometry and the method based on the surface roughness. The first one is a classical method of the literature (used by Sun et al. [27], for example) to estimate the teeth formation frequency and the dispersion on it depends on the dispersion on the undeformed tooth length. The second has, to the authors' knowledge, not been employed so far. It presents the advantage to require only a surface roughness measurement system, allowing to get significant results quickly. The dispersion on the teeth formation frequency estimated by this method is, moreover, very low. Future studies could consider other cutting speeds and depths of cut values to apply and validate the methods proposed to estimate the teeth formation frequency for other cutting conditions.

## Conclusions

Ti6Al4V strictly orthogonal cutting experiments were performed on a DMU-80T high speed milling machine. This unique setup uses the milling machine as a planer: the tool is fixed on the table and the sample, inserted into the spindle, moves horizontally at the cutting speed. Four different values of the depth of cut were considered. The forces were measured and the chips were collected to be observed under a microscope after etching.

For the depth of cut of 280 $\mu$m, the chip was saw-toothed. The teeth shape was regular, allowing a rigorous exploitation of their lengths. The microstructure analysis of the chips showed that the Ti6Al4V chip formation came from the deformation and the propagation of a crack inside the primary shear zone for the cutting conditions of this paper. The digital microscope highlighted that there was no material between the teeth on the lateral faces of the chip. Macroscopically, this resulted in a kind of "lateral milling" of the chip.

Measured forces confirmed that the cut was orthogonal (the mean value of the lateral force is zero). The forces level decreased with the depth of cut as expected and their evolutions were cyclic for the saw-toothed chip.

Reducing the depth of cut led to a continuous chip (at 100 $\mu$m and 60 $\mu$m), then continuous with small teeth (at 40 $\mu$m). The forces also exhibit an evolution with the depth of cut. They decreased with it, as expected, and the feed to cutting forces ratio increased with it, showing the non-negligible influence of the tool edge radius for small depths of cut.

The arithmetic roughness of the machined surface was similar for all of the depths of cut (and low in the context of machining by removing chips) except for 280 $\mu$m. In this case, the roughness was higher and the measured profile had a cyclic evolution.

The teeth formation frequency was estimated by the chip morphology, the evolution of the cutting force (FFT and the least squares) and the roughness of the machined surface. Except for the geometry leading to a slightly higher frequency, the other methods resulted in very similar values to each other, around 2100 Hz (the roughness method had the lowest standard deviation).

These experiments can now be used to validate the results of 2D plane strain numerical models of Ti6Al4V in orthogonal cutting. The comparison could be performed on the chip morphology (without chip distortion due to unrolling), the chip formation mechanism, the forces and the teeth formation frequency. The simplicity of the experimental setup and the near-to-zero investments it requires makes it suitable to be widely used for other materials in order to provide a strong benchmark for the validation of numerical orthogonal cutting models, as long as the cutting speed is compatible with the feed rate of the machine and the maximum cutting force does not get too close to the overload protection of the spindle.

**Acknowledgments** The authors gratefully acknowledge Technofutur Industrie for making their experimental resources available to us; the Metallurgy Department of the UMONS Faculty of Engineering for making their microstructure analysis resources available to us; Prof. P. Lambert from the *Université Libre de Bruxelles* for the high speed camera; and Dr F. Dagrain from the Department of Structural Mechanics of the UMONS Faculty of Engineering for giving us the opportunity to make some chip observations under the Keyence digital microscope.

## References

1. Altintas Y (2012) Manufacturing automation metal cutting mechanics machine tool vibrations, and CNC design. Cambridge University Press
2. Bai Y, Dodd B (1992) Adiabatic shear localisation occurrence theories and applications. Pergamon Press

3. Bäker M, Rosler J, Siemers C (2002) A finite element model of high speed metal cutting with adiabatic shearing. Comput Struct 80:495–513. doi:10.1016/S0045-7949(02)00023-8
4. Bouchnak TB (2010) Study of extreme stress behavior and machinability of a new aeronautical titanium alloy: the ti555-3. Arts et Métiers ParisTech - Centre de Angers, PhD thesis
5. Calamaz M, Coupard D, Girot F (2008) A new material model for 2D numerical simulation of serrated chip formation when machining titanium alloy Ti-6Al-4V. Int J Mach Tools Manuf 48:275–288. doi:10.1016/j.ijmachtools.2007.10.014
6. Chevalier A (2003) Guide du dessinateur industriel. Hachette Technique
7. Combres Y (2013) Propriétés du titane et de ses alliages, Editions T.I.
8. Combres Y, Champin B (2013) Traitements thermiques des alliages de titane, Editions T.I.
9. Destefani J (1990) Introduction to titanium and titanium alloys, properties and selection nonferrous alloys and special-purpose materials, vol 2. ASM Handbook
10. Ducobu F, Rivière-Lorphèvre E, Filippi E (2011) A lagrangian FEM model to produce Saw-toothed Macro-chip and to study the depth of cut influence on its formation in orthogonal cutting of Ti6Al4V. Adv Mater Res 223:3–11. doi:10.4028/www.scientific.net/AMR.223.3
11. Ducobu F, Rivière-Lorphèvre E, Filippi E (2013) Chip formation in Micro-cutting. J Mech Eng Autom 3:441–448
12. Ducobu F, Rivière-Lorphèvre E, Filippi E (2014) Numerical contribution to the comprehension of saw-toothed Ti6Al4V chip formation in orthogonal cutting. Int J Mech Sci 81:77–87. doi:10.1016/j.ijmecsci.2014.02.017
13. Ezugwu E, Wang Z (1997) Titanium alloys and their machinability – a review. J Mater Process Technol 68:262–274. doi:10.1016/S0924-0136(96)00030-1
14. Fourment L, Delalondre F (2008) A 3D study of the influence of friction on the adiabatic Shear Band formation during High Speed Machining, Proceedings of the ESAFORM2008 Conference. doi:10.1007/s12289-008-0101-5
15. Gammon L, Briggs R, Packard J, Batson K, Boyer R, Domby C (2004) Metallography and microstructures of titanium and its alloys. Metallography and Microstructures, ASM Hanbook, vol 9, pp 899–917
16. Gey N (1997) Étude des changements de textures par transformation de phase $\beta \rightarrow \alpha$ dans des produits TA6V laminés chaud. PhD thesis, Université de Metz
17. Hua J, Shivpuri R (2004) Prediction of chip morphology and segmentation during the machining of titanium alloys. J Mater Process Technol 150:124–133. doi:10.1016/j.jmatprotec.2004.01.028
18. Jousset H (2008) Viscoplasticity and microstructures of a titanium alloy : effects of temperature and strain rate. PhD thesis, École des Mines de Paris
19. Komanduri R (1982) Some clarifications on the mechanics of chip formation when machining titanium alloys, Wear, vol 76, pp 15–34. doi:10.1016/0043-1648(82)90113-2
20. Lampman S (1990) Wrought Titanium and Titanium Alloys, Properties and Selection: Nonferrous Alloys and Special-Purpose Materials, vol 2. ASM Handbook
21. Mahnama M, Movahhedy M (2010) Prediction of machining chatter based on FEM simulation of chip formation under dynamic conditions. Int J Mach Tools Manuf 50:611–620. doi:10.1016/S0749-6419(01)00003-1
22. Molinari A, Musquar C, Sutter G (2002) Adiabatic shear banding in high speed machining of Ti-6Al-4V experiments and modeling. Int J Plast 18:443–459. doi:10.1016/S0749-6419(01)00003-1
23. Owen D, Vaz M (1999) Computational techniques applied to high-speed machining under adiabatic strain localization conditions. Comput Methods Appl Mech Eng 171:445–461. doi:10.1016/S0045-7825(98)00220-5
24. Pantalé O, Bacaria JL, Dalverny O, Rakotomalala R, Caperaa S (2004) 2D and 3D numerical models of metal cutting with damage effects. Comput Methods Appl Mech Eng 193:4383–4399. doi:10.1016/j.cma.2003.12.062
25. SECO TOOLS (2011) Turning catalog and technical guide 2012. SECO TOOLS AB
26. Sima M, Özel T (2010) Modified material constitutive models for serrated chip formation simulations and experimental validation in machining of titanium alloy Ti-6Al-4V. Int J Mach Tools Manuf 50:943–960. doi:10.1016/j.ijmachtools.2010.08.004
27. Sun S, Brandt M, Dargusch M (2009) Characteristics of cutting forces and chip formation in machining of titanium alloys. Int J Mach Tools Manuf 49:561–568. doi:10.1016/j.ijmachtools.2009.02.008
28. The ASM Handbook Committee (1997) Fatigue and Fracture Properties of Titanium Alloys, vol 2, 10th. ASM International
29. The French Titanium Association (2013) The french titanium association Titanium a material for the biomedical industry. http://www.titane.asso.fr/biomedical-eng.html
30. The French Titanium Association (2013) The french titanium association Markets and applications. http://www.titane.asso.fr/markets-and-applications.html
31. Vyas A, Shaw MC (1999) Mechanics of saw-tooth chip formation in metal cutting. J Manuf Sci Eng 121:163–172. doi:10.1115/1.2831200
32. Wan Z, Zhu Y, Liu H, Tang Y (2012) Microstructure evolution of adiabatic shear bands and mechanisms of saw-tooth chip formation in machining Ti6Al4V. Mater Sci Eng A 531:155–163. doi:10.1016/j.msea.2011.10.050
33. Ye G, Chen Y, Xue F, Dai L (2014) Critical cutting speed for onset of serrated chip flow in high speed machining. Int J Mach Tools Manuf 86:18–33. doi:10.1016/j.ijmachtools.2014.06.006
34. Zhang Y, Mabrouki T, Nelias D, Gong Y (2011) FE-model for titanium alloy (Ti-6Al-4V) cutting based on the identification of limiting shear stress at tool-chip interface. Inter J Mater Forming 4:11–23. doi:10.1007/s12289-010-0986-7